Modeling of a Surface Acoustic Wave Strain Sensor

W. C. Wilson*, G. M. Atkinson**

*NASA Langley Research Center, Hampton, VA, USA, w.c.wilson@larc.nasa.gov
**Virginia Commonwealth University, Richmond, VA, USA, gmatkins@vcu.edu

ABSTRACT

NASA Langley Research Center is investigating Surface Acoustic Wave (SAW) sensor technology for harsh environments aimed at aerospace applications. To aid in development of sensors a model of a SAW strain sensor has been developed. The new model extends the modified matrix method to include the response of Orthogonal Frequency Coded (OFC) reflectors and the response of SAW devices to strain. These results show that the model accurately captures the strain response of a SAW sensor on a Langasite substrate. The results of the model of a SAW Strain Sensor on Langasite are presented.

Keywords: Surface Acoustic Wave, SAW, strain, modeling, Langasite.

1 INTRODUCTION

NASA's Integrated Vehicle Health Monitoring (IVHM) project is investigating new detection technologies that will increase aviation safety by monitoring the structural health of aerospace vehicles during flight. These new technologies must be rugged, light weight and low power. Surface Acoustic Wave (SAW) devices are low power, small and make extremely sensitive sensors for performing a variety of measurements [1]. SAW sensors can be designed to be small passive wireless sensors that are capable of operation in harsh environments like those found inside of aerospace structures. A new SAW strain sensor model has been created that aids in the development of prototype passive SAW strain sensors.

Figure 1 is a diagram of a simple SAW sensor that employs four OFC reflectors in two banks. RF energy collected by the antenna is transformed from electrical energy into mechanical waves in the surface of the material by the interdigital transducer (IDT). The waves travel across the substrate and impinge upon the reflector gratings. Since the OFC reflectors divide up the frequency bandwidth of the IDT, and each one reflects a different piece of the bandwidth, OFC systems are very efficient. The OFC reflectors have minimal interference with each other when compared to single frequency reflector systems that use time delay encoding. In the time delay encoding, each reflector reduces the amount of energy available for the next reflector in the same reflector bank.

Multiple OFC reflector gratings are used in each bank to give a unique code to each sensor and to incorporate spread spectrum communications for robust operation in multipath RF environments. Bidirectional IDTs are often used with two sets of reflector banks spaced such that the time response from each bank does not overlap. This allows a large number of reflectors to be used for unique identification of the device and for spread spectrum types of communications.

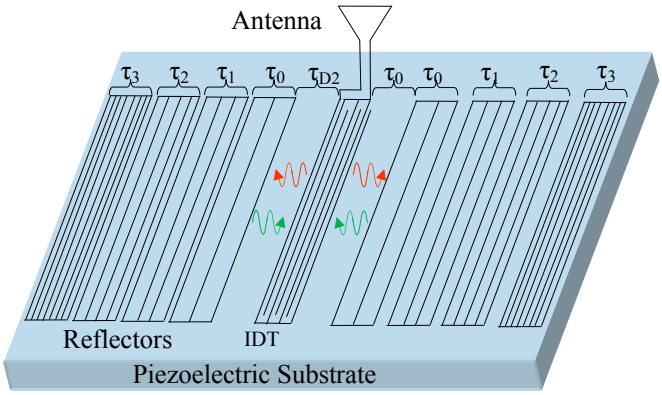

Fig. 1. SAW sensor with four OFC reflectors and antenna. Surface acoustic waves traveling in the material are represented by the red and green arrows.

2 ORTHOGONAL FREQUENCY CODING MODELING

Previously, different methods for modeling SAW devices have been compared [2]. The modified matrix model provides the best results for a single frequency device like a delay line or filter. OFC devices use multiple frequencies in a spread spectrum technology manner [3]. The modified matrix models have been extended to include the response of OFC grating reflectors. A prototype design has been developed that has two reflector banks. Each reflector bank is comprised of four sets of gratings. The four grating sets have frequencies of 301.19, 303.47, 305.75, 308.03 MHz. The reflectors banks are positioned on either side of an interdigitated transducer with spacing such that the reflections do not overlap in time. The prototype design is used as an example in this work. The four separate frequencies used in both reflectors banks are shown in Fig. 2. To meet the constraints of orthogonality, the peak of each frequency occurs at the null for all of the others. This will allow the mechanical wave energy to pass through reflectors that do not match the reflector frequency

criteria and be reflected only by a corresponding reflector. This aspect of OFC reflectors allows for more consistent amplitude and maximum efficiency of returned energy from the reflector gratings that comprise a reflector bank.

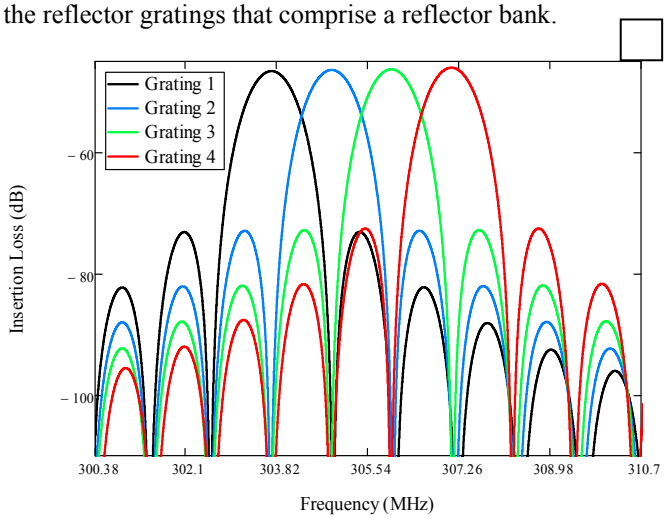

Fig. 2. Frequency Response of each OFC Grating.

The response for a single grating is found using the same techniques as the transmission line matrix for an IDT and is explained in the modified matrix method [2]. The grating transmission matrix for a shorted reflector grating is a sub-matrix of the IDT transmission line matrix and is given by [4]

$$G(f)=\begin{bmatrix} g_{11} & g_{12} \\ g_{21} & g_{22} \end{bmatrix}=\begin{bmatrix} t_{11} & t_{12} \\ t_{21} & t_{22} \end{bmatrix}. \tag{1}$$

Where G is the grating transmission matrix, and g are sub-elements for the grating matrix, *t* are the sub-elements from the modified IDT transmission matrix. The reflection coefficient (*S* parameter) S_{11} is given by

$$S_{11}(f)=\frac{g_{21}}{g_{11}}. \tag{2}$$

The reflection coefficient response of all eight gratings are combined together, taking into account the time delay for each grating to give the total frequency response of the device. The total S_{11} response is given by:

$$S_{11}(f)_{total}=-\sum_{i=1}^{n} S_{11}(f)_i e^{-j2\pi f d_i \tau_i}. \tag{3}$$

Where S_{11} is the single port reflection S parameter, f is the frequency, d_i is the delay for each reflector with respect to the IDT, τ_i is the time length of each reflector, and n is the number of reflectors (eight for this example).

The number of fingers in each grating is 261, 264, 265, 268, which gives is the time length of each reflector (τ_i) of 0.8601, 0.8634, 0.8635, and 0.87 μs each. The metallization thickness used in the model is 0.15 μm. The four gratings have frequencies of 301.19, 303.47, 305.75, 308.03 MHz arranged in order f1, f2, f3, f4, with f1 closest to the IDT. More diverse arrangements of the frequencies that make up a reflector bank would allow for more code diversity when uniquely identifying the sensor in a multisensory environment [5]. Langasite ($La_3Ga_5SiO_{14}$) was chosen for the substrate because it has the potential for high temperature operation. Langasite does not have any phase transitions up to its melting point, which means it does not lose its piezoelectric properties until 1470 °C [6]. This property makes it very attractive for harsh environment locations such as are found in aerospace applications. Langasite crystal with an Euler orientation of (0, 138.5, 26.6) was used for modeling, it has a Rayleigh velocity of 2741 m/s.

The reflectors banks are positioned on either side of an interdigitated transducer with spacing such that the reflections do not overlap in time. The reflectors are shorted, meaning that for each grating the fingers are connected on the top and bottom through metal bus bars. The reflector gratings for each frequency are electrically isolated from each other. The delay to the beginning of the closest reflector bank is 0.860122 μs or τ_0. The time length of the reflector bank (τ_B) is just the sum of the individual time lengths for each frequency grating, and is given by

$$\tau_B=\tau_0+\tau_1+\tau_2+\tau_3. \tag{5}$$

The time length of the reflector banks are τ_B = 3.4571 μs long. The second reflector bank is farther away from the IDT than the first bank. The spacing can be given in terms of a time delay, therefore the delay time for the sencond reflector bank (τ_{D2}) is given by

$$\tau_{D2}=2\tau_0+2\tau_B. \tag{6}$$

The second reflector bank time delay (τ_{D2}) is 5.177 μs. The first reflector bank is delayed by τ_0 from the IDT. The second bank is delayed by the round trip time of two times τ_0 and twice the time length of the first reflector bank to insure that the reflected signals do not overlap in time.

The insertion loss of the frequency response is usually converted into decibels, and given by:

$$IL(f)=-20\log(|S_{11}(f)_{total}|). \tag{4}$$

Where $IL(f)$ is the frequency dependent insertion loss, from the $S_{11}(f)_{total}$ parameter. Using the prototype parameters given earlier, the insertion loss for a device with two sets of gratings that correspond to those in Fig. 2 can be calculated. The results shown in red in Fig. 3.

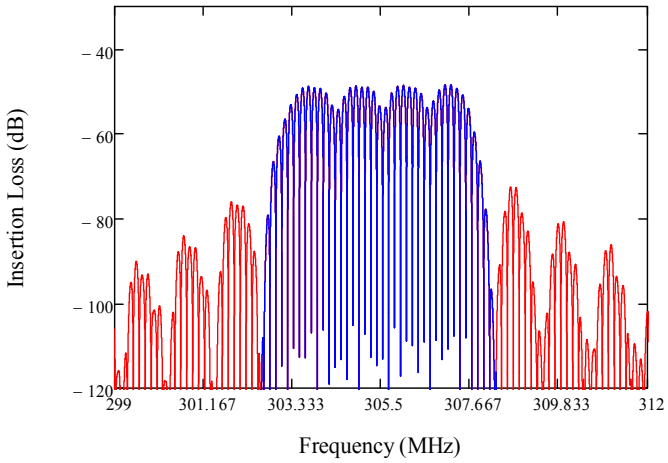

Fig. 3. Frequency Response of all eight OFC gratings combined (red), and the subsection used for cross correlation (blue).

3 STRAIN DETECTION METHOD

When tension causes an elongation of a SAW device the finger widths and spacing both increase causing the frequency of operation to decrease. Similarly when compression causes the finger widths and spacing to be reduced, this causes the frequency to increase. This change in frequency is proportional to the amount of strain. Therefore, the change length which causes a change in frequency is used for this modeling effort to detect strain.

There are multiple ways to detect a change of frequency; one way is to use cross correlation to compare a baseline frequency spectrum to the current spectrum. Correlation is often used in communication systems and SAW sensors systems [7]. It can be performed in either the time or frequency domain [8]. The cross correlation function used on the frequency data in the model is given by:

$$R_{xx}(\tau) = \sum_{n} x_n \bar{x}_{n-\tau} \tag{5}$$

where R_{xx} is the discrete cross correlation, x_n is the original signal, and $\bar{x}_n$ is the complex conjugate of x, and τ is the lag for each signal point.

The model requires a baseline measurement be taken in a calibration procedure, but is simple and relatively fast. A subset of the baseline measurement is gated to capture the main response of the reflector banks and then cross correlated against the measurement data. The use of this subset baseline measurement instead of an ideal response will account for higher order effects found in real-world systems. The baseline signal and the gated subset response are shown in blue in Fig. 3. The results of cross correlation that correspond to three cases of elongation (0nm, 5.5nm, 11.1nm) are shown in Fig. 4.

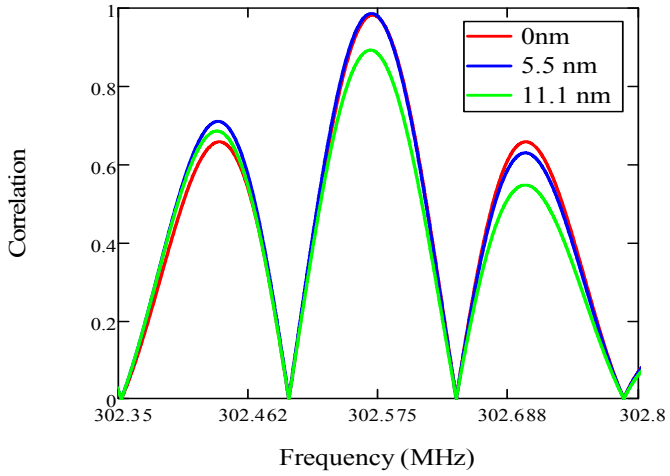

Fig. 4. Correlation peaks for three elongation values.

The maximum peaks in Fig. 4 occur at 302.5700 MHz, 302.5691 MHz, and 302.5682 MHz for 0nm, 5.5nm, 11.1nm respectively. There are three peaks due to the two identical banks of reflectors. When the cross correlation is performed the minor peaks occur when the gated signal matches one of the reflector banks to the measured signal.

The maximum peak occurs when both of the reflector banks in the gated signal match both of the reflector banks in the measured signal. Note that for the center peak there is a change in amplitude for the case of 11.1nm but not for the case of 5.5nm. There is however, are change of frequency for both cases, even though it is very hard to see the small shift in frequency between the 0nm and 5.5nm cases. This is why frequency rather than amplitude is used within the model.

4 RESULTS

The results from the model are in the form of correlation values that relate to a frequency spectrum for a particular case. The next step is to find the peaks in each correlation and reference the frequency that corresponds to those peaks. The peak frequency for one elongation case is used as the baseline. The other values are subtracted from the baseline to yield the frequency shift. The frequency shifts are multiplied by a conversion factor to change them from Hertz (Hz) to micro strain (με). The conversion factor used for the model is 0.017666 με s. The units for the conversion factor are micro strain seconds. The final results are micro strain. For this example, the model was used to provide the strain caused by elongation from 0nm to 11.1nm in 0.9 nm increments, which corresponds to 0 με to 3.152 με, in ~0.262 με increments.

The model needs to extremely accurate if it is to be used to develop SAW strain sensors on high temperature substrates. Sensors have been previously developed with principal strain sensitivity of 13 nano strain on ZnO substrates[9]. The results show that the model accurately

captures the strain response of a SAW OFC strain sensor on a Langasite wafer as compared to the expected linear relationship between strain and elongation (Fig. 5). The results agree very closely and differ by only a negligible amount (on the order of 10^{-16}).

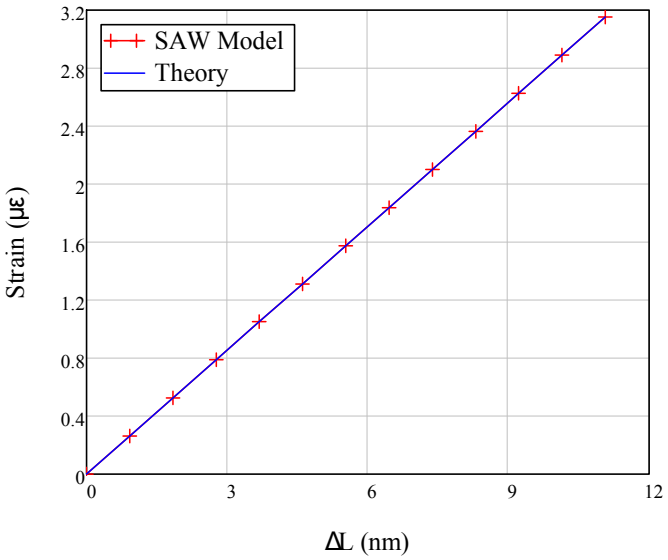

Fig. 5. SAW simulation results compared to the expected value.

There is very little information that can be derived from Fig 5. More insight into the accuracy of the model is given in Fig. 6, a plot of the difference between the expected value and model's value. The model values agree with the theory to within $5x10^{-16}$ without linearization.

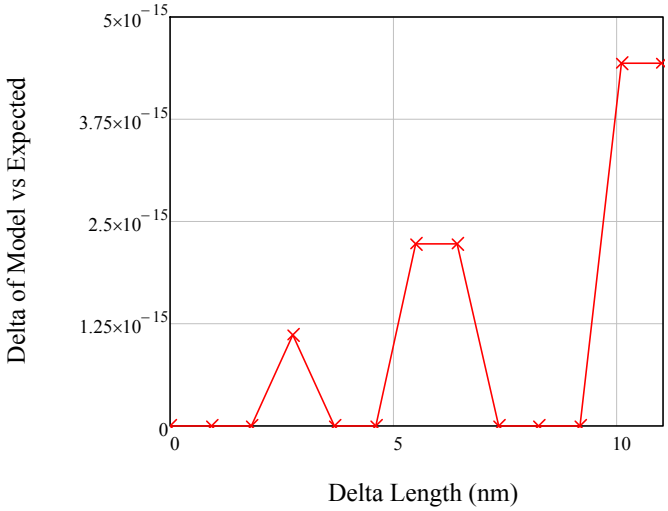

Fig. 6. Plot of the difference values between the expected strain and the SAW model strain values.

5 CONCLUSIONS

The results from the development of a SAW sensor model that incorporates OFC reflectors and strain response are presented. The results from the model are compared to theory for strain from elongation. These results show that the model accurately captures the strain response of a SAW sensor on Langasite versus the theory. The model values agree with the theory to within $5x10^{-16}$ without linearization.

Prototype devices are being developed to compare and validate the models. Future work will also include characterization of the prototype for temperature effects. These effects could then be incorporated into the model.

REFERENCES

[1] W. C. Wilson, *et al.*, "Orthogonal Frequency Coded SAW Sensors for Aerospace SHM Applications," *Sensors Journal, IEEE,* vol. 9, pp. 1546-1556, Nov. 2009.

[2] W. Wilson and G. Atkinson, "Comparison of Transmission Line Methods for Surface Acoustic Wave Modeling," *Sensors & Transducers Journal,* vol. 7, pp. 150 - 159, October 2009.

[3] J. M. Pavlina, *et al.*, "SAW RFID Spread Spectrum OFC and TDM Technology," in *RFID, 2009 IEEE International Conference on*, Orlando, FL, 2009, pp. 110 -116.

[4] H. Y. Tung, "The Design of Surface Acoustic Devices using the Transmission Matrix Method," Ph.D Dissertation, I-Shou University, 2005.

[5] D. Malocha, *et al.*, "Ultra Wide Band Surface Acoustic Wave (SAW) RF ID Tag and Sensor," in *Military Communications Conference, 2009. MILCOM 2009. IEEE*, 2009, pp. 1-7.

[6] J. Hornsteiner, *et al.*, "Surface Acoustic Wave Sensors for High-Temperature Applications," in *Frequency Control Symposium, 1998. Proceedings of the 1998 IEEE International*, 1998, pp. 615-620.

[7] D. R. Gallagher and D. C. Malocha, "Ultra Wide Band SAW Correlators using Dual Orthogonal Frequency Coded Transducers," in *Frequency Control Symposium, 2009 Joint with the 22nd European Frequency and Time forum. IEEE International*, Besancon, France, 2009, pp. 24-27.

[8] H. Zhu, *et al.*, "Application of PRO-ESPRIT Algorithm in Identification of Surface Acoustic Wave Identification-Tags," *Journal of Shanghai University (English Edition),* vol. 12, pp. 347-351, 2008.

[9] M. D. G. Potter, *et al.*, "Low cost thin film based surface acoustic wave vibration sensors for vibrational gyroscope," in *Frequency Control Symposium and PDA Exhibition, 2002. IEEE International*, 2002, pp. 220-224.